RSC Advances

ROYAL SOCIETY OF CHEMISTRY

www.rsc.org/advances

Application of ordered mesoporous silica nanocontainers in anticorrosive epoxy coating on magnesium alloy surface

Yingjie Qiao*[a], Wenpeng Li[b], GuixiangWang*[a], Xiaohong Zhang[a], Nana Cao[a]

[a] *Key Laboratory of Superlight Materials and Surface Technology, Ministry of Education, College of Materials Science and Chemical Engineering, Harbin Engineering University, Harbin, 150001, China*

[b] *Institute of Materials, China Academy of Engineering Physics，Mianyang 621700，China*

1. Introduction

Magnesium alloys are the lightest structural materials with excellent physical and mechanical properties, such as low density (it is only 65% that of aluminium and 25% that of iron), high strength/weight ratio, excellent castability, machinability and damping characteristic.[1-3] These advantages makes them very attractive to plenty of fields, including automotive, cellular phones, computer industry, aircraft and guided weapons industries.[4] On the contrary, magnesium and its alloys are poor to corrosion resistance and will be easily oxidized to form a loose oxide film (MgO and $Mg(OH)_2$) on the surface because of their high chemical activity and low electrode potential.[5]

Among the technical applications developed to protect the magnesium alloys from corrosion, sol-gel coatings, which have good adhesion to the metal, good barrier property for corrosion protection, low treatment temperatures and simple fabrication process, are the most common and cost effective method.[6-8] In recent years, hybrid organic-inorganic sol-gel coatings that contain inorganic salts, organic corrosion inhibitors or nanoparticles are paid more and more attention. However, the incorporation of these compounds depressed the coherence of the coating matrix which resulted in reduced corrosion protection. In order to overcome these disadvantages, various

types of nanocontainers were used to encapsulate the corrosion inhibitors.

The nano hollow particles often exhibit unique properties from those of common particles, such as large surface area, high pore volume, low density, stability and non-toxic nature.[9-10] This is making them be paid more and more attention in scientific and technological fields. In recent years, surface anti-corrosion coatings that contained cerium molybdate nanocontainers or TiO_2 nanocontainers loaded with corrosion inhibitors were used on aluminum alloys surface,[11-12] hot dip galvanised steel surface,[13-14] and magnesium alloys surface.[15-16] The total impedance values of these coatings as a function of time was measured after exposure in corrosive environment, and found that the enhancement properties of the containing loaded nanocontainers coatings was due to a possible self-healing effect.

As the diameter and position of the containers are important factors influencing anticorrosion efficiency of the coatings, some researcher prepared water-based organic coating on the surface of aluminium alloy substrates containing corrosion inhibitor loaded different size of silica nanocontainers. They found that the self-healing performance was increased by adding smaller diameter containers and decreasing the distance between nannocontainers and metal surface.[17-18] In addition, pH value could also affect the release of inhibitors from the nanocontainers and proved the self-healing properties of the coatings.[19-20] And 2-Mercaptobenzothiazole (MBT) was usually selected to be loaded to nanocontainers due to its corrosion inhibitor properties.[21-22]

In the present work, magnesium alloy were coated via a dip-coating process with an epoxy sol-gel coating that contained ordered mesoporous silica nanocontainers loaded with 2-mercaptobenzothiazole (MBT). Anti-corrosion properties of these coatings were conducted by EIS in NaCl solution. Moreover, Transmission electron microscopy (TEM), thermogravimetric analysis (TGA) and Fourier transform infrared (FTIR) spectra were used to the structure and component analysis.

2. Materials and methods

2.1. Materials

Magnesium alloy samples (with dimension of 25 mm×25 mm×5 mm), epoxy resin and amino hardener were prepared from company. 2-Mercaptobenzothiazole xylene, n-butanol, ammonia solution, tetraethoxysilane, hexadecyl trimethyl ammonium bromide and sodium chloride were analytical grade reagents. These reagents were used without further purification.

2.2. Preparation of SiO_2 nanocontainers and encapsulation of inhibitors

Ordered mesoporous SiO_2 nanocontainers were synthesized and then loaded with anodic corrosion inhibitor MBT, according to literature.[23-24] Firstly, CTAB was added into mixed solution of $NH_3 \cdot H_2O$ and triple distilled water, and the solution were sonicated for 10 min. Then TEOS was added dropwisely into the above homogeneous mixture and the reaction was kept at 30^{o}C for 1 h with a constant magnetic stirring. After reaction, the collected product was centrifuged, repeatedly washed with water to remove surfactants. And then, the sample was dried at 80^{o}C for overnight. After dry-

ing, the sample was heat treated in air in a muffle furnace at 550^{o}C for 3 h to burn off the organic surfactant.

The MBT loaded silica nanocontainers were obtained by stirring 0.5 g SiO_2 in 50 mL acetone saturated solution of MBT under vacuum conditions for 1 h. Then, the silica nanocontainers loaded with MBT were collected through centrifugation and drying under vacuum at 60^{o}C for 12 h.

2.3. Preparation of coatings

The composition of the epoxy solution is presented in table 1.

Initially, n-butanol and xylene were mixed together. Then, the appropriate amount of silica loaded nanocontainer was added to the above solution (solution A), under ultrasonic treatment for 2 min. After that, epoxy resin and amino hardener were dissolved in solution A (solution B). Before the dip coating process, the solution B was magnetically stirred with high speed for 40 min, and then was transferred to a vacuum chamber for 20 min to remove the air bubble.

The magnesium alloy samples were dip coated into the epoxy solution for four times with a low withdraw rate after 2 min immersion. After that, the coated panels were cured at room temperature for 24 h initially, and then were heat treated at temperature 60^{o}C for 2 h.

Two different coatings were prepared, one including 2% w/w (loaded nanocontainers/(epoxy + hardener)) MBT loaded nanocontainers (Epoxy-2 wt.% silica-MBT

coating), the other including 4% w/w MBT loaded nanocontainers (epoxy-4 wt.% silica-MBT coating). Moreover, the corresponding coatings including empty nanocontainers (Epoxy-2 wt.% silica coating, Epoxy-4 wt.% silica coating), the coating including MBT (Epoxy-MBT coating) and the coating without any additives were prepared.

2.4. Characterization

The optical coating photographs of the coatings were determined by metallo-scope using Leicadmirm (Leica Company) microscope.

Fourier transform infrared (FTIR) spectra were recorded on a Perkin Elmer Spectrum 100 spectrometer, which were obtained in the range of 4000-450 cm^{-1} at a resolution of 4 cm^{-1} by casting a thin film on a KBr plate for the coatings.

The corrosion resistance of these coatings was studied via electrochemical impedance spectroscopy (EIS) using a CHI760E electrochemical workstation. The experiments were performed at room temperature in a three electrode cell, where the sample, a platinum sheet and a saturated calomel electrode (SCE) were the working, the counter and the reference electrode, respectively. All the potentials were referred to the SCE. A sample area of 1 cm^2 was exposed to NaCl solution, and the electrochemical measurements of the samples were measured at different immersion time. The measuring frequency of EIS ranged from 10^5 Hz down to 10^{-2} Hz, with sinusoidal alternating potential signal of 10 mV. The EIS spectra of the samples were fitted using the ZSimpWin software.

The nanocontainer powder XRD patterns were recorded on TTRIII diffractometer using Cu κ_α radiation. The diffraction data were recorded in the 2θ range of 1–8°. Nitrogen adsorption/desorption measurements were conducted using SSA-5000 by N_2 physisorption at 77 K to examine the specific surface areas of the nanocontainers. Transmission electron microscopy (TEM) was performed on a FeiTecnia G2-STWIN at 220 kV to examine the morphology of the silica nanocontainers. The loading of the corrosion inhibitor into the containers was estimated by thermogravimetric analysis (TGA) using TA instruments Q50 at a heating rate of 20 °C min^{-1} under a nitrogen atmosphere at a flow rate of 50 mL min^{-1}.

3. Results and discussion

3.1. Ordered mesoporous silica nanocontainers

Fig. 1 displays the small-angle XRD pattern of the silica nanocontainers synthesized following the above procedure. As shown in this figure, a well-resolved peak and two small peaks can be indexed as the diffraction planes (100), (110) and (200), which present a typical characteristic of MCM-41.[25] Thus, the lattice spacing was calculated 3.92 nm according to Bragg's equation with a hexagonal structure plane of (100) peak at 2θ＝2.25°. This result indicates that well-ordered mesoporous structures have been formed according to the above synthetic method. TEM micrographs (Fig. 2) also show clearly that highly ordered pore structure has been synthesized, where the size distribution of silica nanocontainers is uniform and the diameter is about 93 nm.

In order to investigate parameters of mesoporous structure, N_2 adsorption/desorption experiment of silica nanocontainers was performed. Specific surface area, pore volume and average hole diameter of the silica nanocontainers was 873.4 m^2 g^{-1}, 0.850 cm^3 g^{-1} and 3.90 nm, respectively.

Fig. 3 shows the TGA curves of pure MBT and silica nanocontainers loaded with MBT. Both spectra of them demonstrate weight loss after 170^{o}C, corresponding to oxidative degradation of MBT. The TGA curve of silica nanocontainer loaded with MBT depicts a sharp weight loss between 200^{o}C and 300^{o}C, which is due to the burn off of MBT that is on the shell of the silica nanocontainers. The other slow weight loss between 300^{o}C and 350^{o}C correspond to the degradation of the MBT that is inside the silica nanocontainers. This result denotes that MBT is encapsulated in the containers. Finally, the SiO_2 nanocontainers are 83.7% (w/w) loaded with MBT inhibitor.

3.2. Corrosion tests

The corrosion protection properties of the coated samples were estimated using EIS. Corrosion test process includes the exposure of the coated panels to 3.5 wt.% NaCl solution at room temperature for 168 h.

Figs. 4-9 present the impedance spectra obtained during 168 h immersion time for epoxy coating, epoxy-MBT coating, epoxy-2 wt.% silica coating, epoxy-4 wt.%

silica coating, epoxy-2 wt.% silica-MBT coating and epoxy-4 wt.% silica-MBT-coating, respectively.

The coating without nanocontainers or inhibitors (epoxy coating) reveals two time constants during the immersion time (Fig. 4). One is in the high frequency range, which can be attributed to barrier properties of the coating film. The other one is in the middle frequency range that can be ascribed to the response of process occurring in the coating/substrate interface.[26] The low frequency impedance values for the coat coating range from 5.6 $M\Omega \cdot cm^2$ to 0.3 $M\Omega \cdot cm^2$. Moreover, penetration phenomenon after 24 h and 120 h immersion is observed in Fig. 4, which is attributed to the penetration in the coating and coating/substrate interface, i.e., the epoxy coating loses its anti-corrosion ability after 120 h immersion.

The corrosion behavior of the coating including inhibitor (epoxy-MBT coating) is depicted in Fig. 5. The Bode spectra also reveal two time constants. One is in the high frequency range due to the coating properties. The other is in the middle frequency range at the initial immersion time, and as the time elapses transfers to low frequency range (~ 0.1 Hz), which can be attributed to the pitting onset. The low frequency impedance values for epoxy-MBT coating range from 6×10^3 $M\Omega \cdot cm^2$ to 30 $M\Omega \cdot cm^2$.

EIS Bode plots of epoxy-2 wt.% silica-coating and epoxy-4 wt.% silica-coating

are demonstrated in Fig. 6 and Fig. 7. The Bode spectra present one time constant due to the coating protection. The low frequency impedance values for coatings range from 1.7×10^4 MΩ·cm^2 to 2.2 MΩ·cm^2 and from 1.5×10^4 MΩ·cm^2 to 3.7 MΩ·cm^2, respectively.

The Bode spectra obtained for the coating including 2 wt.% loaded nanocontainers (epoxy-2 wt.% silica-MBT coating) are presented in Fig. 8. It reveals two time constants, which can be attributed to the anticorrosion properties of the film and the coating/substrates interface. The low frequency impedance values for the coating range from 8.3×10^3 MΩ·cm^2 down to 1.4 MΩ·cm^2.

Fig. 9 shows the response of the coating with SiO_2 nanocontainers loaded with MBT as a function of time. The phase angle is between -80^o to -70^o at the immersion time of 24 h revealing that the coating behaves as a capacitor and acts as an insulator. [27]As the immersion time goes on, one time constant in high frequency range is appeared due to the coating protection, and then another time constant around 1 Hz is also appeared associated to the coating/substrate interface response. The low frequency impedance values for the coating range from 1.9×10^5 MΩ·cm^2 down to 24.2 kΩ·cm^2.

It can be noticed that the low frequencies impedance values of epoxy coating, epoxy-2 wt.% silica-coating, epoxy-2 wt.% silica-MBT coating and epoxy-4 wt.% silica-MBT coating are increased in different degree at the initial immersion time, suggesting possible self-healing effect.[28]

The Bode plots of the EIS spectra obtained for all the coated samples after 24 h of immersion time are depicted in Fig. 10. It can be clearly observed from the impedance values at the low frequency range that epoxy-4 wt.% silica-MBT coating demonstrates the best anticorrosion properties after 24 h immersion time as its value is increased compared to other coatings. It should be noticed that the epoxy-4 wt.% silica-MBT coating presents better anticorrosion properties than the epoxy-2 wt.% silica-MBT coating. Moreover, the coatings of epoxy coating, epoxy-MBT coating and epoxy-2 wt.% silica-MBT coating present two constants, which can be attributed to barrier properties and coating/substrate interface. This result reveals that the epoxy-2 wt.% silica-MBT coating does not improve the anticorrosive properties compared to the epoxy-4 wt.% silica-MBT coating. A possible explanation could be the lower release rate of MBT inhibitor from epoxy-2 wt.% silica-MBT coating after the appearance of coating defects.

Detailed interpretation of the EIS measurements was performed by numerical simulation with equivalent electrical circuit models. Fig. 11 shows four equivalent circuits used in this study. The constant phase element (CPE) was used instead of an

ideal capacitor to simulate capacitive response of the Bode plots.

The resistance of the solution is illustrated as R_s. The epoxy coating is simulated by the equivalent circuit of Fig. 11d after 24 h and 120 h immersion time, while by the equivalent circuit of Fig. 11c at other immersion time. The epoxy-MBT coating is simulated by the equivalent circuit of Fig. 11c. The circuits of epoxy-2 wt.% silica coating and epoxy-4 wt.% silica coating is presented by Fig. 11b, which includes one time constant. The equivalent circuit for the epoxy-2 wt.% silica-MBT coating is Fig. 11c. The epoxy-4 wt.% silica-MBT coating presents a capacitive response after 24 h immersion time (Fig. 11a) and is simulated by the equivalent circuit of Fig. 11b after 12 h, 48 h and 72 h immersion time. As the immersion time goes on, two time constants appeared and the appropriate fitting circuit is Fig. 11c.

All coated samples of fitting parameters (R_{coat} and C_{coat}) are presented in Fig. 12 during the immersion time in corrosive environment. The results reveal that the coatings with additives present less capacitive behavior during the immersion time. Furthermore, the epoxy-4 wt.% silica-MBT coating exhibits the least capacitive values during the middle immersion time. The epoxy coating presents the less resistance values, which comes in accordance with the capacitance results. The resistance values of coating including 2 wt.% empty silica nanocontainers or coating containing loaded nanocontainers tend to increase during the initial immersion and decrease with the elapse of immersion time due to electrolyte uptake and formation of conductive

pathways.[29] The possible explanation of the results may also own to self-healing effect.[28]

Moreover, it is noticed that the epoxy-4 wt.% silica-MBT coating exhibits the highest resistive values between 24 h and 48 h immersion time. Thus, the incorporation of 4 wt.% silica nanocontainers loaded with MBT has the better anticorrosion properties.

In order the possible self-healing properties to be evaluated, artificial detects of 2 mm were created on the surface of the epoxy coating, epoxy-4 wt.% silica coating and epoxy-4 wt.% silica-MBT coating. Then the coated samples were exposed to 0.1 mol/L NaCl solution at room temperature. Fig. 13 depicts the EIS Bode spectra of epoxy coating acquired after 4 days of immersion. Although a decrease of the impedance values in the low frequency range is observed during the first day, there is increase of impedance values after 24 h immersion. Similar behavior is observed for the coating containing 4 wt.% loaded silica nanocontainers (Fig. 15). It should be noticed that the impedance values of epoxy-4 wt.% silica coating in the low frequency does not increase with the immersion time elapses (Fig. 14).

Both epoxy coating and epoxy-4 wt.% silica coating reveal one time constant in

the high frequency range due to the film before 24 h immersion. Then, another time constant is appeared in the middle frequency range after 48 h immersion due to the penetration of electrolytes in the corrosive environment. Thus, the EIS results of epoxy coating and epoxy-4 wt.% silica coatings after the formation of defect were fitted by the equivalent circuit of Fig. 8b before 24 h immersion, and then by the equivalent circuit of Fig. 8c. The epoxy-4 wt.% silica-MBT coating was fitted by the equivalent circuit of Fig. 8c. Fig. 16 depicts the evolution of R_{coat} and C_{coat} as a function of time in 0.1 mol/L NaCl solution for the coatings after formation of the defect. As shown in the fitting results, the R_{coat} values of the epoxy-4 wt.% silica-MBT coating decrease at the initial immersion time, but the R_{coat} values are slightly increased after 10 h immersion and after 48 h immersion. The similar behavior is observed for the epoxy coating. However, the R_{coat} values of epoxy-4 wt.% silica coating always decrease with increasing the immersion time. One of the self-healing definitions is the partial recovery of the protective properties of the coating system.[30] Thus, the results denote that only both epoxy coating and epoxy-4 wt.% silica-MBT coating are being partially recovered from artificial defects and suggest both coatings probably have self-healing properties.

The possible self-healing properties of the samples can be explained as in Fig.17. When chloride ions (Cl^-) migrate to the magnesium/epoxy coating interface, the formation of magnesium hydroxide will release hydroxide ions to increase local area pH. The reaction between amine group and epoxy groups is catalyzed by increased pH to

produce a new protective film.[13, 31] Thus, the epoxy coating presents the self-healing property. The disappearance of self-healing property of the epoxy-4 wt.% silica coating may be caused by the concentration of the silica nanocontainers, which hindered the reaction between epoxy and ammine group. As the pH value changes with the formation of magnesium hydroxide, the partial recovery of the epoxy-4 wt.% silica-MBT coating can be attributed to the sustainable released MBT inhibitor from the silica nanocontainers during immersion in the corrosive environment.[32, 33]

3.3. FT-IR spectroscopy analysis

The FT-IR spectra of the epoxy coating, epoxy-4 wt.% silica coating and epoxy-4 wt.% silica-MBT coating are depicted in Fig. 18 (a), (b) and (c), respectively. The adsorption peak at 947 cm^{-1} in Fig. 18b corresponds to Si-OH stretching band[34] and demonstrates that silica nanocontainers have been encapsulated in the coating. The FT-IR spectrum of epoxy-4 wt.% silica-MBT coating (Fig. 18c) shows adsorption peaks at 694 cm^{-1}, 765 cm^{-1} (C-S stretching vibrations) and 3041 cm^{-1} (phenyl ring C-H stretching vibrations), which reveals that loaded silica nanocontainers have been encapsulated in the epoxy coating.[35] The O-H stretching vibrations are depicted around 3402 cm^{-1}. The peaks around 2930 cm^{-1} is related to the C-H brand vibration of epoxy resin. The adsorption bands at 1300 cm^{-1}, 1458 cm^{-1}, 1513 cm^{-1} and 1611 cm^{-1} correspond to the amino hardener group vibrations.[11] The peak at 1247 cm^{-1} is related to the epoxy ether band. The peaks at 1180 cm^{-1}, 1035 cm^{-1} and 833 cm^{-1} are

due to the aromatic carbon vibration of epoxy resin.[36] The peak around 1096 cm^{-1} corresponds to C-N band of amino hardener.[37] The peak at 565 cm^{-1} is related to C-phenyl out of plane ring deformation vibration of epoxy resin.[11] It should be noticed that an intense peak at 1760 cm^{-1} only appears in Fig. 18c, which is attributed to C=O band of CO_2 in the air.[38]

The results observed above revealed that hybrid organic-inorganic epoxy coatings including nanocontainers or loaded nanocontainers had successfully prepared on the surface of magnesium alloy.

3.4. Morphology of the coatings

The optical photographs of samples before and after exposure to 3.5 wt.% NaCl solution for 168 h are presented in Fig. 19. Before exposure to corrosive environment, the surface of epoxy coating (Fig. 19a) presents wavy morphology. The surface of epoxy-MBT coating (Fig. 19c) occur lots of hole with the addition of MBT inhibitors, which may become the penetration channel of corrosive electrolyte. With the addition of nanocontainers (Fig. 19e and Fig. 19g), the surfaces of these coatings are no macroscopic defects, and the less concentration of nanocontainers, the surface of coatings looks more smooth. Same behavior is observed on the surface of the coatings containing loaded nanocontainers (Fig. 19i and Fig. 19k).

The surface of epoxy coating and epoxy-MBT coating damaged mostly after 168 h exposure to corrosive environment (Fig. 19b and Fig. 19d). They are coarse

with lots of distinct holes. However, the surfaces of coatings containing empty nanocontainers present less corrosion hole and look largely intact (Fig. 19f and Fig. 19h). These results reveal that the anticorrosion property is improved by addition silica nanocantiners. Interestingly, the surfaces of coatings containing MBT loaded nanocontainers present snowflake-shaped cracks but no corrosive holes (Fig. 19j and Fig. 19l). Moreover, the crack reduces with the increase of the concentration of MBT loaded nanocontainers. This phenomenon can be ascribed to the release of MBT inhibitor when microcracks occur on the surface of the loaded nanocontainers encapsulated coatings, which inhibits the generation of corrosion holes. The results demonstrate that the coatings containing MBT loaded nanocontainers have self-healing properties.

4. Conclusions

In this research, a system including hybrid organic-inorganic epoxy coating has been synthesized for the corrosion protection of magnesium alloy. Furthermore, SiO_2 nanocontainers loaded with MBT inhibitors or empty nanocontianers were incorporated into the coating. Their corrosion resistance was examined using EIS. The results showed improved corrosion protection during the immersion process in 3.5 wt.% NaCl solution.

The concentration of loaded nanocontainers into the coating is an important factor for the anticorrosion property of the coatings. The coating containing 4 wt.%

loaded nanoncontainers presented the highest impedance values after 24 h immersion in the corrosive environment and showed partial recovery action after artificial defects exposure to corrosive environment. Otherwise, the coating containing 4 wt.% nano-containers didn't present partial recovery action. These results demonstrate the self-healing properties of the coatings containing MBT loaded nanocontainers on the surface of magnesium alloy.

Acknowledgements

The authors gratefully acknowledge the financial support of NSFC 51479037, 51305090, Innovation Talent Research Fund of Harbin Science and Technology (RC2014QN015006), and Fundamental Research Funds for the Central Universities (HEUCF20151010).

References

1 J. E. Gray and B. Luan, *J. Alloys Compd.*, 2002, **336**, 88.

2 H. Friedrich and S. Schumann, *J. Mater. Process. Tech.*, 2001, **117**, 276.

3 H. Altun and S. Sen, *Mater. Design.*, 2004, **25**, 637.

4 A. K. Sharma, R. Uma Rani and S. M. Mayanna, *Thermochim. Acta*, 2001, **376**, 67.

5 F.H. Froes, D. Elieser and E. Aghion, *The Minerals Metals & Materials Society*, 1998, **5**, 30.

6 F. Deflorian, S. Rossi, M. Fedel and C. Motte, *Prog. Org. Coat.,* 2010, **69**, 158.

7 C.Y. Tsai, J.S. Liu, P.L. Chen and C.S. Lin, *Corros. Sci.*, 2010, **52**, 3907.

8 J.B. Bajat, V.B. Miskovic-Stankovic, J.P. Popic and D.M. Drazic, *Prog. Org. Coat.*,

2008, **63**, 201.

9 P.P. Yang, S.L. Gai and J. Lin, *Chem. Soc. Rev.*, 2012, **41**, 3679.

10 R. Rostamiana, M. Najafic and A. A. Rafati, *Chem. Eng. J.,* 2011, **171**, 1004.

11 I. A. Kartsonakis, A.C. Balaskas and G.C. Kordas, *Corros. Sci.*, 2011, **53**, 3771.

12 A.C. Balaskas, I.A. Kartsonakis, L.A. Tziveleka and G.C. Kordas, *Prog. Org. Coat.*, 2012, **74**, 418.

13 I.A. Kartsonakis, A.C. Balaskas, E.P. Koumoulos, C.A. Charitidis and G.C. Kordas, *Corros. Sci.*, 2012, **57**, 30.

14 M.F. Montemor, D.V. Snihirova, M.G. Taryba and S.V. Lamaka, *Electrochim. Acta*, 2012, **60**, 31.

15 I.A. Kartsonakis, E.P. Koumoulos, C.A. Charitidis and G. Kordas, *J. Nanopart. Res.*, 2013, **15**, 1.

16 I.A. Kartsonakis, A.C. Balaskas, E.P. Koumoulos and C.A. Charitidis, *Prog. Org. Coat.*, 2013, **76**, 459.

17 D. Borisova, D. Akçakayıran, M. Schenderlein, H. Möhwald and D. G. Shchukin, *Adv. Funct. Mater.*, 3013, **23**, 3799.

18 D. Borisova, H. Möhwald and D.G. Shchukin, *ACS Appl. Mater. Inter.*, 2012, **5**, 80.

19 M. Saremi and M. Yeganeh, *Corros. Sci.*, 2014, **86**, 159.

20 J.M. Falcón, F.F. Batista and I.V. Aoki, *Electrochim. Acta*, 2014, **124**, 109.

21 B. Sanyal, *Prog. Org. Coat.*, 1981, **9**, 165.

22 M.L. Zheludkevich, K.A. Yasakau, S.K. Poznyak and M.G.S. Ferreira, *Corros.*

Sci., 2005, **47**, 3368.

23 M. Najafi, Y. Yousefi and A.A. Rafati, *Sep. Purif. Tehcnol.*, 2012, **85**, 193.

24 I.A. Kartsonakis and G. Kordas, *J. Am. Ceram. Soc.*, 2010, **93**, 65.

25 D. Borisova, H. Möhwald and D.G. Shchukin, *ACS Nano*, 2011, **5**, 1939.

26 M.F. Montemor and M.G.S. Ferreira, *Electrochim. Acta*, 2007, **52**, 6976.

27 W. Trabelsi, E. Triki, L. Dhouibi, M.G.S. Ferreira, M.L. Zheludkevich and M.F. Montemor, *Surf. Coat. Tech.*, 2006, **200**, 4240.

28 D.G. Shchukin, S.V. Lamaka, K.A. Yasakau, M. L. Zheludkevich, M. G. S. Ferreira and H. Möhwald, *J. Phys. Chem. C*, 2008, **112**, 958.

29 D. Snihirova, S.V. Lamaka and M.F. Montemor, *Electrochim. Acta*, 2012, **83**, 439.

30 M.F. Montemor, R. Pinto and M.G.S. Ferreira, *Electrochim. Acta*, 2009, **54**, 5179.

31 E.V. Skorb and D.V. Andreeva, *Polym. Chem.*, 2013, **4**, 4834.

32 M.D. Wang, M.Y. Liu and J.J. Fu, *J. Mater. Chem. A*, 2015, **3**, 6423.

33 J.J. Fu, T. Chen, M.D. Wang, N.W. Yang, S.N. Li, Y. Wang and X.D. Liu, *ACS Nano*, 2013, **7**, 11397.

34 A. Fidalgo and L.M. Ilharco, *J. Non-cryst. Solids*, 2001, **283**, 144.

35 X.H. Li, Z.X. Tang and X.Z. Zhang, *Spectrochim. Acta A Mol. Biomol. Spectrosc.*, 2009, **74**, 168.

36 A. Cherdoud-Chihani, M. Mouzali and M.J.M. Abadie, *J. Appl. Polym. Sci.*, 2003, **87**, 2033.

37 S.S. Golru, M.M. Attar and B. Ramezanzadeh, *Prog. Org. Coat.*, 2014, **77**, 1391.

1 38 L. Song, S. Xuan, X. Wang and Y. Hu, *Thermochim. Acta*, 2012, **527**, 1.

Figures:

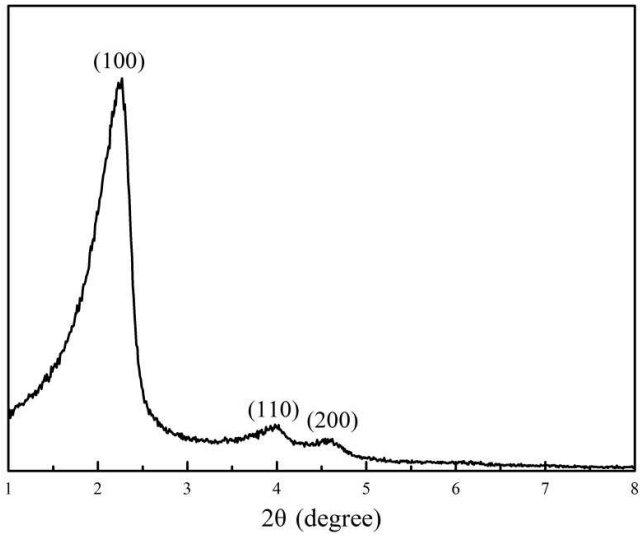

Fig. 1. XRD pattern of silica nanocontainers.

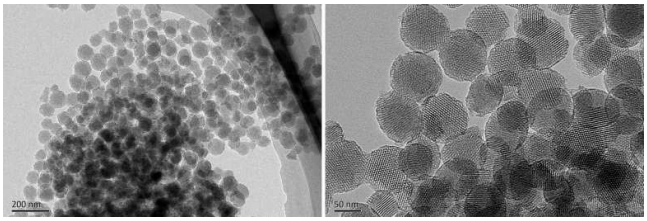

Fig. 2 TEM micrographs of silica nanocontainers.

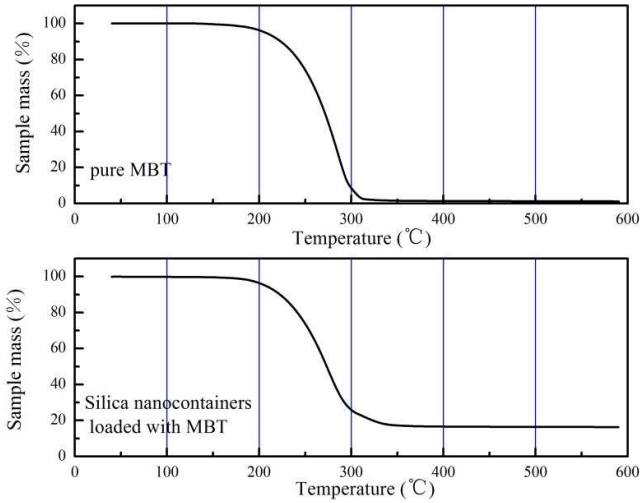

Fig. 3 TGA curves of pure MBT and silica nanocontainers loaded with MBT.

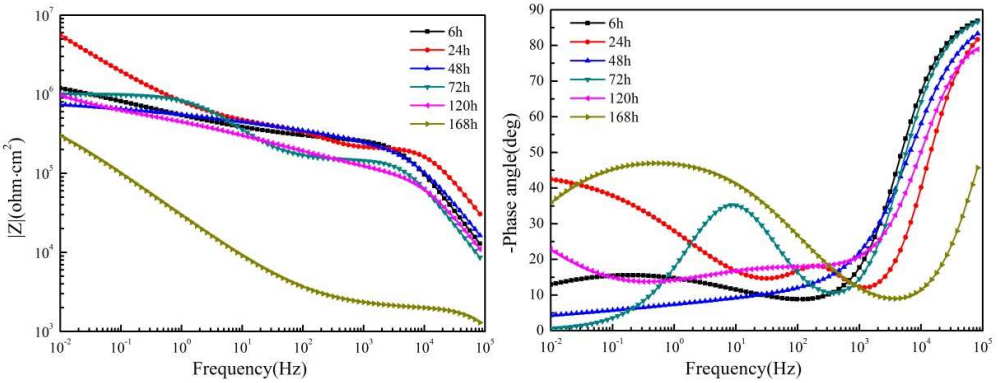

Fig. 4 EIS Bode plots of epoxy coating after exposure to 3.5 wt.% NaCl solution for different immersion time.

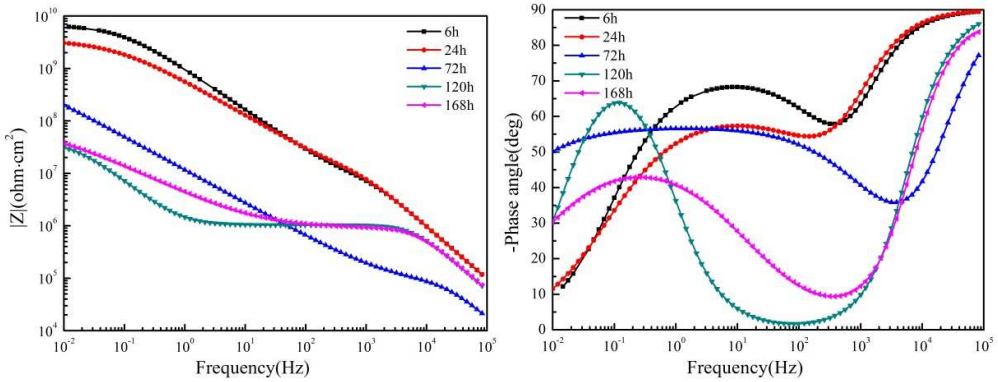

Fig. 5 EIS Bode plots of epoxy-MBT coating after exposure to 3.5 wt.% NaCl solution for different immersion time.

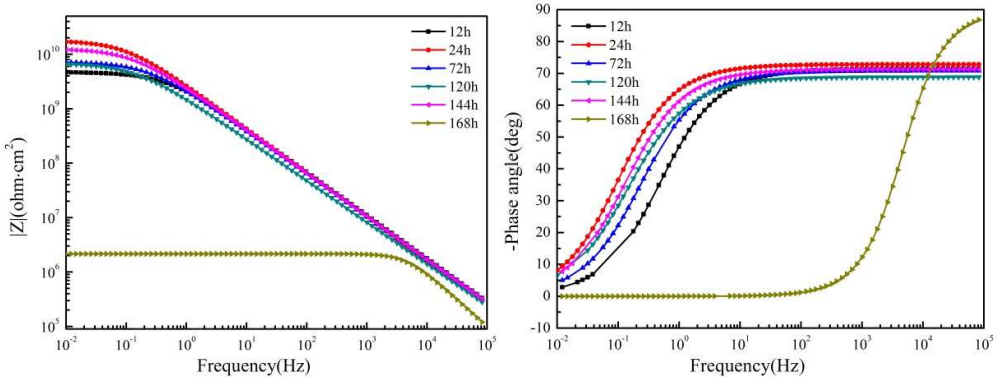

Fig. 6 EIS Bode plots of epoxy-2 wt.% silica coating after exposure to 3.5 wt.% NaCl solution for different immersion time.

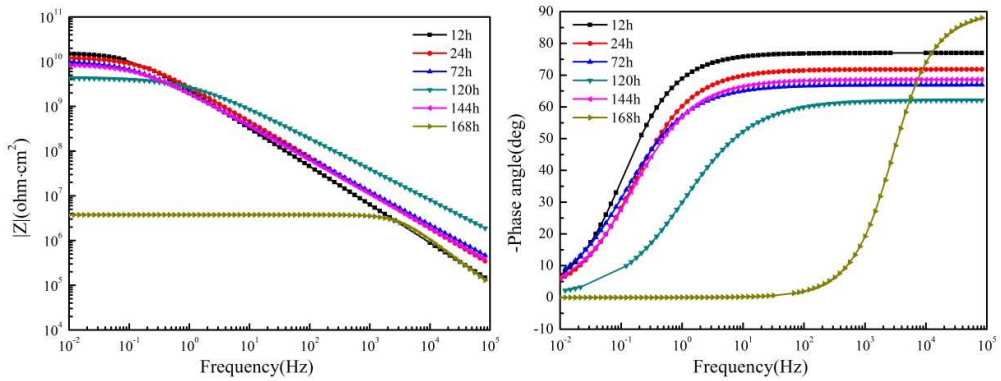

Fig. 7 EIS Bode plots of epoxy-4 wt.% silica coating after exposure to 3.5 wt.% NaCl solution for different immersion time.

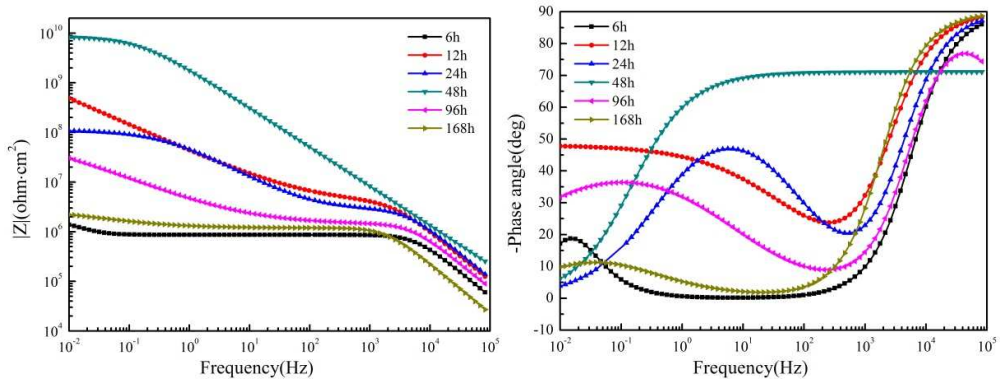

Fig. 8 EIS Bode plots of epoxy-2 wt.% silica-MBT coating after exposure to 3.5 wt.% NaCl solution for different immersion time.

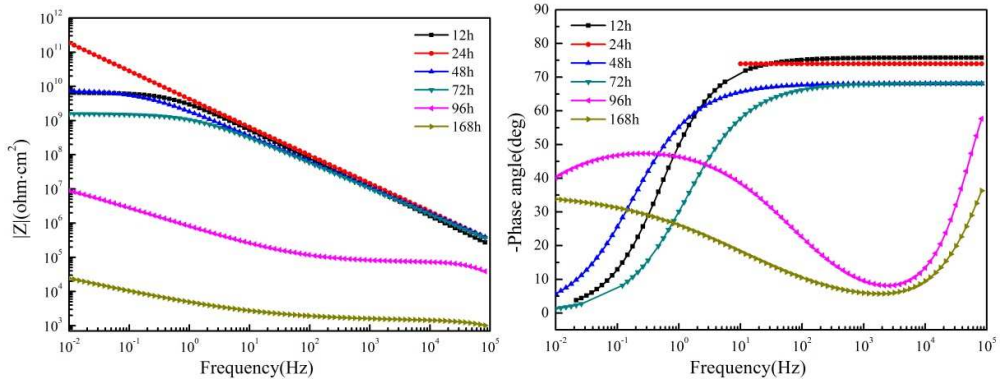

Fig. 9 EIS Bode plots of epoxy-4 wt.% silica-MBT coating after exposure to 3.5 wt.% NaCl solution for different immersion time.

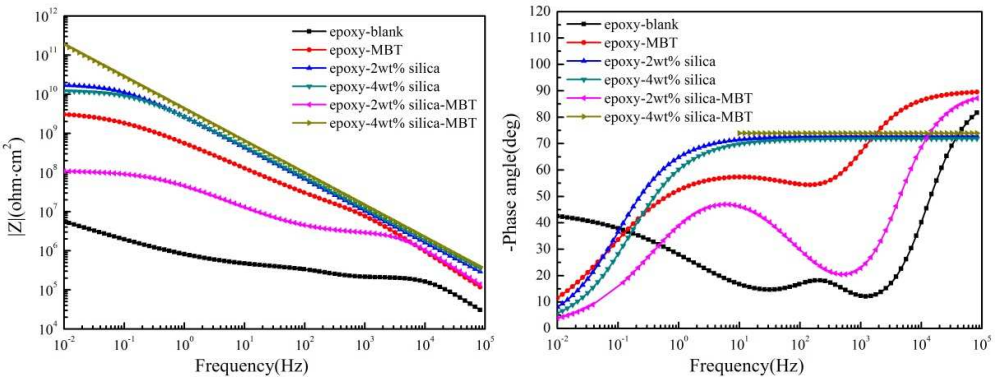

Fig. 10 Bode plots of all coated samples after exposure to 3.5 wt.% NaCl solution at room temperature for 24 h.

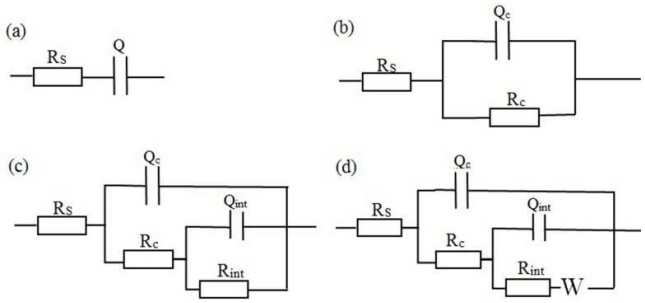

Fig. 11 Equivalent circuits used for the fitting of the EIS measurements.

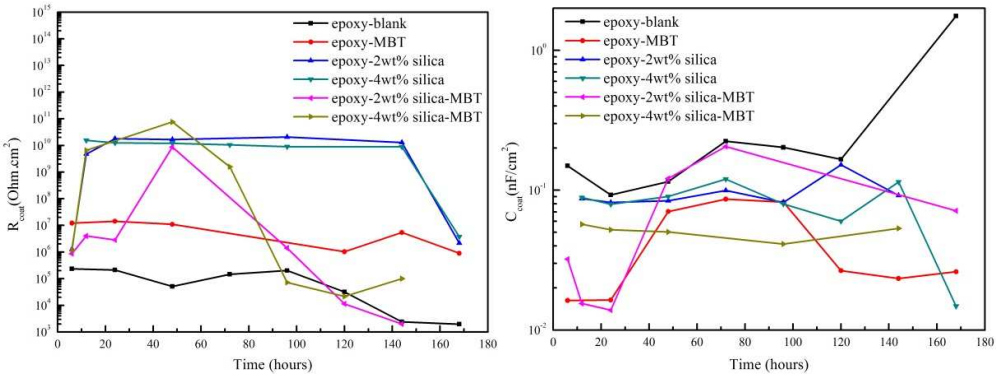

Fig. 12 R_{coat} and C_{coat} evolution of all coated samples as a function of time after exposure to 3.5 wt.% NaCl solution at room temperature.

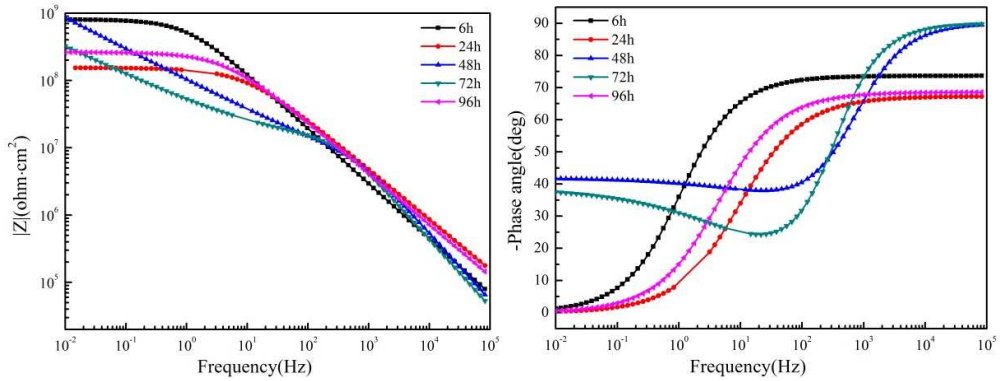

Fig. 13 Bode plots of epoxy coating after artificial defect exposure to 0.1 mol/L NaCl solution.

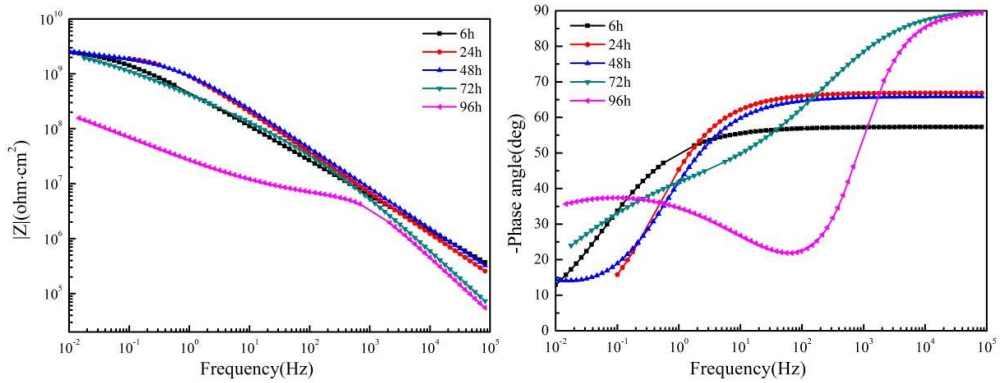

Fig. 14 Bode plots of epoxy-4 wt.% silica coating after artificial defect exposure to 0.1 mol/L NaCl solution.

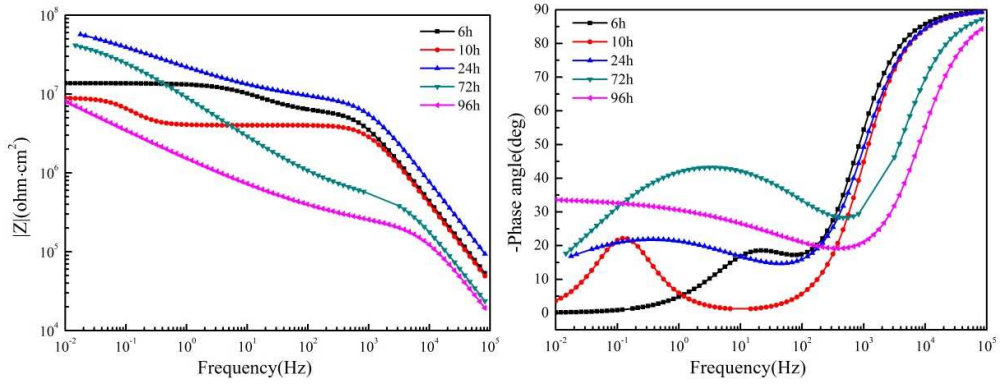

Fig. 15 Bode plots of epoxy-4 wt.% silica-MBT coating after artificial defect exposure to 0.1 mol/L NaCl solution.

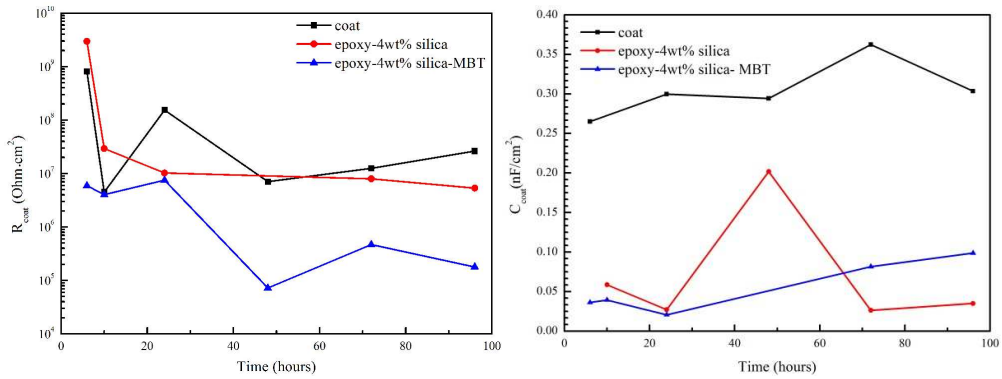

Fig. 16 Evolution of the Bode fitting parameters as a function of time in 0.1 mol/L NaCl solution for the defected coating.

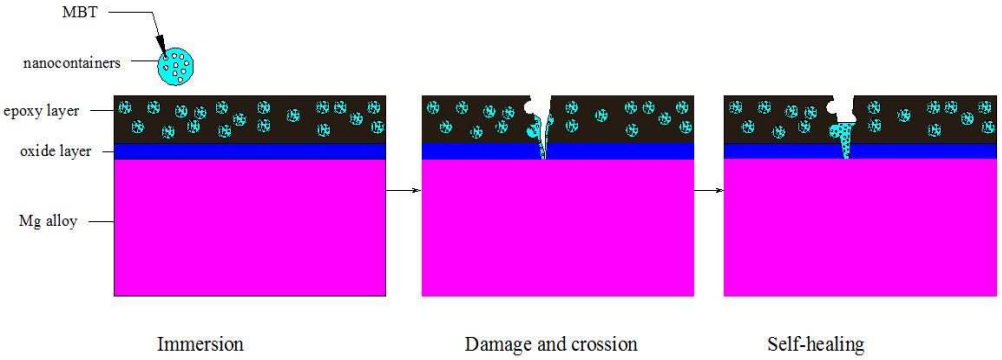

Fig. 17 A schematic representation of self-healing properties of the coatings

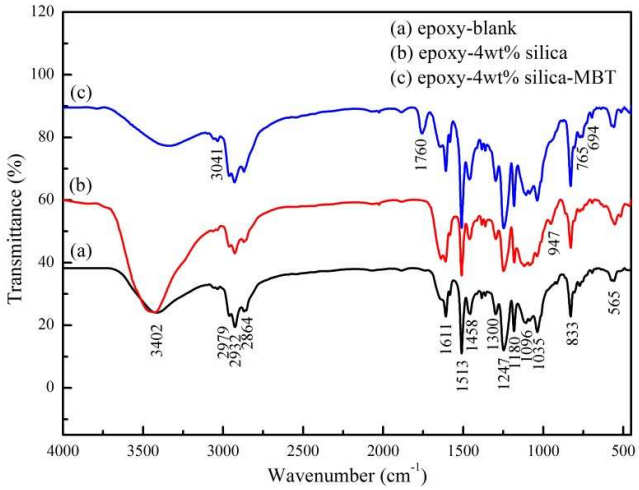

Fig. 18 FT-IR spectra of epoxy coating, epoxy-4 wt.% silica coating and epoxy-4 wt.% silica-MBT coating.

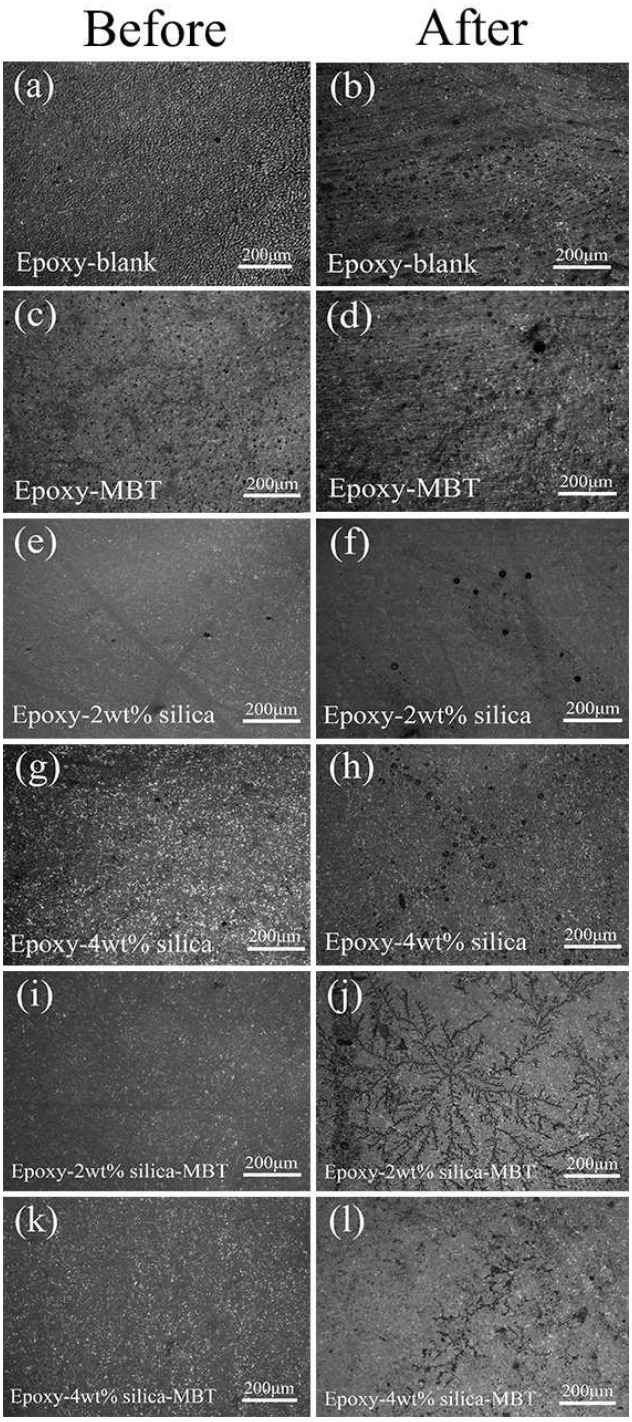

Fig. 19 Surface morphology of coatings before and after exposure to 3.5 wt.% NaCl solution for 168 h.

Table 1

Reagents used for the preparation of epoxy solution.

Materials	epoxy resin	hardener	n-butanol	xylene
Quantity (g)	20	4.74	1.5	3.5